



Efficient numerical simulation of fractional extended Heston models including interest rate driven by variable-order Brownian motions

Zahra Tokasi¹, Mousa Ilie^{1,*}, Behrouz Parsa Moghaddam², and Kamyar Hosseini^{3,4}

¹Department of Mathematics, Ra.C., Islamic Azad University, Rasht, Iran.

²Department of Mathematics, La.C., Islamic Azad University, Lahijan, Iran.

³Department of Mathematics, Near East University TRNC, Mersin 10, Nicosia 99138, Turkey.

⁴Faculty of Engineering and Natural Sciences, Istanbul Okan University, Istanbul, Turkey.

Abstract

This research introduces an innovative and computationally efficient methodology for examining fractional extended Heston models that incorporate interest rate within the framework of variable-order Brownian motions. The approach employs trapezoidal quadrature techniques to approximate both the fractional integral and the associated stochastic fractional systems, providing a robust numerical foundation. A comprehensive convergence analysis validates the proposed scheme's mathematical soundness and reliability. The methodology's accuracy and convergence characteristics are rigorously evaluated against established function integration methods from the existing literature, establishing its comparative advantages and limitations. Building upon this theoretical framework, the developed approach is applied to solve these sophisticated models, revealing important insights into how stochastic effects influence stock price dynamics. The investigation extends further to analyze crucial statistical indicators for determining the optimal fractional order within the interval (0.5,1), using genetic algorithms. The research also explores various parametric configurations of the variable-order Hurst index within the range [0.5,1), providing deeper insights into the model's behavior under different conditions. The results show that the fractional Heston-Cox-Ingersoll-Ross model with time-varying Hurst index reduces the all error criteria examined in this study compared to fixed Hurst models.

Keywords. Fractional calculus, Fractional extended Heston model, Fractional Brownian motion, Trapezoidal quadrature.

1991 Mathematics Subject Classification. 26A33, 60G22, 91G80, 65D30.

1. INTRODUCTION

Fractional differential equations (FDEs) are powerful tools for investigating numerous phenomena in applied sciences. These equations have been extensively studied in various fields, including epidemic modeling [32], finance [4], image processing [38], and engineering [39]. The existence and uniqueness of solutions for FDEs have been explored in works such as [16, 23, 33]. Moreover, numerous analytical and numerical methods have been proposed to solve various FDEs, including approaches using Chebyshev polynomials [1], Hermite wavelets [12], Hermite interpolation [26], spline interpolation [20, 24] and spectral element [5].

Stochastic differential equations (SDEs) incorporate one or more stochastic terms, leading to solutions based on stochastic processes. The simulation of SDEs with fractional Brownian motion (fBm) has been extensively investigated both theoretically and numerically [2, 6, 18, 19, 22].

Stochastic fractional differential equations (SBFDEs), which arise from fractional Brownian motion (fBm), represent a new branch of mathematics based on fractional calculus. This area has garnered significant attention from researchers [3, 13]. In recent years, many applications of fractional calculus of arbitrary degrees have been developed. These advancements, combined with the development of numerical methods, have enhanced the role of this branch of

Received: 18 August 2025 ; Accepted: 24 October 2025.

* Corresponding author. Email: Mousa.ilie@iau.ac.ir.

mathematics in various sciences, including demographics [35], biology [27], stock price modeling [36], and pollutant transport [28, 29]. Despite extensive theoretical and practical research, obtaining analytical solutions for SBFDEs remains challenging. Therefore, developing efficient numerical approaches for solving SBFDEs continues to be an intriguing and important area of research.

We consider the following *stochastic fractional differential equation in fractional Brownian motion* (SBFDE) in this article:

$$\begin{cases} {}^C \mathcal{D}_{0,t}^\varrho x(t) = \Theta(t, x(t)) + \widehat{\Theta}(t, x(t)) \frac{dW(t)}{dt} + \widetilde{\Theta}(t, x(t)) \frac{d\beta^{H(t)}(t)}{dt}, \\ x(0) = x_0, \end{cases} \quad (1.1)$$

where $\Upsilon := [0, T]$, $\frac{1}{2} < \varrho < 1$, and $\Theta, \widehat{\Theta}, \widetilde{\Theta} : \Upsilon \times \mathbb{R} \rightarrow \mathbb{R}$ are measurable functions. Here, $W(t)$ represents the standard Wiener process.

We apply the Caputo fractional derivative [9, 10], defined as:

$${}^C \mathcal{D}_{0,t}^\varrho x(t) = \int_0^t \frac{(t-\varsigma)^{q-\varrho-1}}{\Gamma(q-\varrho)} x^{(q)}(\varsigma) d\varsigma, \quad 0 \leq q-1 < \varrho \leq q \in \mathbb{N}, \quad (1.2)$$

where the unknown function $x(t)$ is $(q-1)$ -times continuously differentiable. It is worth mentioning that the Caputo derivative, used in Eq. (1.2), is selected because it handles initial conditions well for financial models.

Moreover, we consider $\beta^{H(t)}(t)$, with $H(t) \in [\frac{1}{2}, 1)$, as fractional Brownian motion (fBm) with Hurst index $H(t)$ [37], defined as:

$$\beta^{H(t)}(t) = \int_0^t \frac{(t-\zeta)^{H(t)-\frac{1}{2}}}{\Gamma(H(t)+\frac{1}{2})} \omega(\zeta) d\zeta, \quad (1.3)$$

where $\omega(t)$ represents Gaussian white noise (Gwn). Notably, fBm reduces to the standard Wiener process when $H(t) = \frac{1}{2}$. Additionally, fractional Gaussian white noise (fGwn) [21] is described as:

$$G^{H(t)}(t) = \frac{d\beta^{H(t)}(t)}{dt}. \quad (1.4)$$

The remainder of the article is organized as follows. In section 2, we suggest an efficient method based on trapezoidal quadrature for discretizing the SBFDE (1.1). The convergence analysis of this scheme is detailed in section 3. To investigate the accuracy of the proposed method, several examples are presented in section 4. Additionally, this section explores the stochastic effects on fractional extended Heston models, considering the optimal fractional order and various cases of variable-order Hurst index. Finally, the concluding remarks are provided in section 5.

2. THEORETICAL RESULTS

This section has two purposes. At the first step, an approximation of the fractional-order integral is yielded. Then, the developed scheme is used to solve SBFDE (see, Eq. (1.1)). Hence, we assume $t_m = m\delta$, where $m = \{0, 1, \dots, r\}$, and $\delta = \frac{T}{r}$ means the uniform step size, and $r \in \mathbb{N}$. Moreover, we suppose a complete probability space as $\mathbb{L}^2(\Omega, \mathcal{F}, \mathbb{P})$, and a mean square integrable function with

$$\|x\|_{ms} := \mathbb{E}(\sqrt{\|x\|^2}),$$

where $\|\cdot\|$ indicates the standard Euclidean norm. Also, we consider the left Riemann-Liouville fractional integral of order ϱ ([34]) which is stated as:

$$\mathcal{J}_{0,t}^\varrho x(t) = \int_0^t \frac{(t-\varsigma)^{\varrho-1}}{\Gamma(\varrho)} \cdot x(\varsigma) d\varsigma, \quad (2.1)$$

where $t, \varrho, \varsigma \in \mathbb{R}^+$ and $\Gamma(\cdot)$ denotes the Gamma function.

To discretize, we need to approximate

$$\mathcal{J}_{0,t_r}^\varrho x(t) = \int_0^{t_r} \frac{(t_r-\varsigma)^{\varrho-1}}{\Gamma(\varrho)} x(\varsigma) d\varsigma$$



$$= \frac{1}{\Gamma(\varrho)} \sum_{m=0}^{r-1} \int_{t_m}^{t_{m+1}} (t_r - \varsigma)^{\varrho-1} x(\varsigma) d\varsigma.$$

For this purpose, we can use the trapezoidal quadrature:

$$\begin{aligned} \mathcal{J}_{0,t_r}^{\varrho} x(t) &\approx \frac{1}{2\Gamma(\varrho)} \sum_{m=0}^{r-1} (x_m + x_{m+1}) \int_{t_m}^{t_{m+1}} (t_r - \varsigma)^{\varrho-1} d\varsigma \\ &= \frac{\delta^{\varrho}}{2\Gamma(1 + \varrho)} \sum_{m=0}^{r-1} ((r - m)^{\varrho} - (r - m - 1)^{\varrho}) (x_m + x_{m+1}). \end{aligned} \tag{2.2}$$

Hence, we obtain

$$\mathcal{J}_{0,t_r}^{\varrho} x(t) \approx \frac{\delta^{\varrho}}{2\Gamma(1 + \varrho)} \sum_{m=0}^{r-1} \alpha_{r,m} x_m, \tag{2.3}$$

where

$$\alpha_{r,m} = \begin{cases} r^{\varrho} - (r - 1)^{\varrho}, & \text{if } m = 0, \\ (r - m + 1)^{\varrho} - (r - m - 1)^{\varrho}, & \text{if } 1 \leq m \leq r - 1. \end{cases} \tag{2.4}$$

Proposition 2.1. Assume that $x(t) \in C^2(\Upsilon)$ is a function, $\varrho > 0$, and $\|x''(t)\|_{\infty} \leq \Xi$ where $\Xi > 0$. The truncation error of (2.3) is bounded such that

$$\|AE_r\| = \left\| \mathcal{J}_{0,t_r}^{\varrho} [x(t)] - \left(\mathcal{J}_{0,t_r}^{\varrho} [x(t)] \right)_{approx} \right\| \leq \frac{r^{\varrho} \Xi}{16\Gamma(\varrho + 1)} \delta^{2+\varrho}. \tag{2.5}$$

Lemma 2.2 ([21]). If γ is an M -Hilbert Schmidt operator and $\gamma : \Upsilon \rightarrow \mathcal{L}_2^0$ satisfies $\int_0^T \|\gamma\|_{\mathcal{L}_2^0}^2 d\varsigma < \infty$, where \mathcal{L}_2^0 is a separable Hilbert space, then

$$\mathbb{E} \left\| \int_0^t \gamma(\varsigma) d\beta^H(\varsigma) \right\|^2 \leq t^{2H-1} \int_0^t 2H \|\gamma\|_{\mathcal{L}_2^0}^2 d\varsigma. \tag{2.6}$$

Proposition 2.3. his proposition establishes an approximation for the fractional integral in Eq. (2.7) and derives an error bound using standard mathematical techniques. Assume that $x(t) \in \mathbb{L}^2(\Omega, \mathcal{F}_t, \mathbb{P})$ and $x(t) \in C^2[t_m, t_{m+1}]$ for $m = 0, 1, \dots, r - 1$, with each $[t_m, t_{m+1}] \in \Upsilon$, $\varrho > \frac{1}{2}$, $H(t) \in [\frac{1}{2}, 1)$, and $\|x''(t)\|_{\infty} \leq \Xi$ where $\Xi > 0$. Then,

$$\mathcal{J}_{0,t_r}^{\varrho} (x(t)G^{H(t)}(t)) \approx \frac{\delta^{\varrho}}{2\Gamma(1 + \varrho)} \sum_{m=0}^r \alpha_{r,m} G_m^{H(t_m)} x_m, \tag{2.7}$$

where $\alpha_{r,m}$ is defined in (2.4). Additionally, the truncation error of (2.7) is bounded such that

$$\begin{aligned} \mathbb{E}[\|AE_r^{H(t)}\|] &= \mathbb{E} \left[\left\| \mathcal{J}_{0,t_r}^{\varrho} [x(t)G^{H(t)}(t)] - \left(\mathcal{J}_{0,t_r}^{\varrho} [x(t)G^{H(t)}(t)] \right)_{approx} \right\| \right] \\ &\leq \frac{r^{\varrho-1+H(t_r)} \Xi}{16\Gamma(\varrho)} \sqrt{\frac{2H(t_r)}{2\varrho - 1}} \delta^{1+\varrho+H(t_r)}. \end{aligned} \tag{2.8}$$

Proof. The approximation of $\mathcal{J}_{0,t_r}^{\varrho} (x(t)G^{H(t)}(t))$ can be obtained similarly to (2.3). For proving the second part, let $x_m(t_m)$ be a function as an approximation of $x(t_m)$ in the subinterval $[t_m, t_{m+1}] \subseteq \Upsilon$, for $m = 0, 1, \dots, r - 1$. Therefore, with an arbitrary value $\nu_m \in (t_m, t_{m+1})$, we have

$$\mathcal{E}_m(t) = x(t_m) - x_m(t_m) = \frac{(t - t_m)(t - t_{m+1})}{2!} x''(\nu_m),$$

thus

$$\mathbb{E} \left[\left\| \mathcal{J}_{0,t_r}^{\varrho} [x(t)G^{H(t)}(t)] - \left(\mathcal{J}_{0,t_r}^{\varrho} [x(t)G^{H(t)}(t)] \right)_{approx} \right\| \right] = \mathbb{E} \left[\left\| \frac{1}{\Gamma(\varrho)} \int_0^{t_r} (t_r - \varsigma)^{\varrho-1} \mathcal{E}(\varsigma) G^{H(t)}(\varsigma) d\varsigma \right\| \right]^2$$



$$\begin{aligned}
&= \mathbb{E} \left[\left\| \frac{1}{\Gamma(\varrho)} \int_0^{t_r} (t_r - \varsigma)^{\varrho-1} \mathcal{E}(\varsigma) d\beta^{H(t)}(\varsigma) \right\|^2 \right] \\
&\leq \mathbb{E} \left[\frac{2H(t_r)t_r^{2H(t_r)-1}}{\Gamma^2(\varrho)} \sum_{m=0}^{r-1} \int_{t_m}^{t_{m+1}} \|(t_r - \varsigma)^{\varrho-1} \mathcal{E}_m(\varsigma)\|^2 d\varsigma \right] \\
&= \frac{2H(t_r)t_r^{2\varrho-2+2H(t_r)}}{(2\varrho-1)(16\Gamma(\varrho))^2} \Xi^2 \delta^4.
\end{aligned}$$

Hence, after some simplifications, we obtain

$$\mathbb{E} \left[\|AE_r^{H(t_r)}\| \right] \leq \frac{r^{\varrho-1+H(t_r)}\Xi}{16\Gamma(\varrho)} \sqrt{\frac{2H(t_r)}{2\varrho-1}} \delta^{1+\varrho+H(t_r)}.$$

□

Corollary 2.4. For $H(t) = \frac{1}{2}$, i.e., the standard Wiener process, we have

$$\mathbb{E}[\|AE_r^W\|] \leq \frac{r^{\varrho-\frac{1}{2}}\Xi}{16\sqrt{2\varrho-1}\Gamma(\varrho)} \delta^{\varrho+\frac{3}{2}}. \quad (2.9)$$

Proposition 2.5. Considering the assumptions of Propositions 2.1 and 2.3, Corollary 2.4, and the following assumptions:

(1) Establishing the Lipschitz condition with respect to the second variables with constants $\theta_1, \theta_2, \theta_3 \in \mathbb{R}^+$:

$$\begin{cases} \|\Theta(t, \xi_1) - \Theta(t, \xi_2)\| \leq \theta_1 \|\xi_1 - \xi_2\|, \\ \|\widehat{\Theta}(t, \xi_1) - \widehat{\Theta}(t, \xi_2)\| \leq \theta_2 \|\xi_1 - \xi_2\|, \\ \|\widetilde{\Theta}(t, \xi_1) - \widetilde{\Theta}(t, \xi_2)\| \leq \theta_3 \|\xi_1 - \xi_2\|, \end{cases}$$

(2) $\Theta(\cdot, 0)$ is \mathbb{L}^2 -integrable;

(3) $\widehat{\Theta}(\cdot, 0)$ and $\widetilde{\Theta}(\cdot, 0)$ are essentially bounded.

The numerical solution of the SBFDE (see Eq. (1.1)) is expressed as

$$x_r = x_0 + \sum_{m=0}^{r-1} \frac{\alpha_{r,m} \delta^\varrho}{2\Gamma(1+\varrho)} \left\{ \Theta(t_m, x_m) + \omega(t_m) \widehat{\Theta}(t_m, x_m) + G_m^{H(t_m)} \widetilde{\Theta}(t_m, x_m) \right\}, \quad (2.10)$$

where $\alpha_{r,m}$ is stated in (2.4).

Here is the revised proof with improved readability and applied mathematics expressions:

Proof. By integrating, the SBFDE (1.1) can be expressed as follows:

$$\begin{aligned}
x(t) &= x_0 + \int_0^t \frac{(t-\varsigma)^{\varrho-1}}{\Gamma(\varrho)} \Theta(\varsigma, x(\varsigma)) d\varsigma + \int_0^t \frac{(t-\varsigma)^{\varrho-1}}{\Gamma(\varrho)} \widehat{\Theta}(\varsigma, x(\varsigma)) dW(\varsigma) \\
&\quad + \int_0^t \frac{(t-\varsigma)^{\varrho-1}}{\Gamma(\varrho)} \widetilde{\Theta}(\varsigma, x(\varsigma)) d\beta^{H(t)}(\varsigma),
\end{aligned} \quad (2.11)$$

or

$$x(t) = x_0 + \mathcal{J}_{0,t}^\varrho \Theta(t, x(t)) + \mathcal{J}_{0,t}^\varrho \left(\widehat{\Theta}(t, x(t)) \frac{dW(t)}{dt} \right) + \mathcal{J}_{0,t}^\varrho \left(\widetilde{\Theta}(t, x(t)) \frac{d\beta^{H(t)}(t)}{dt} \right). \quad (2.12)$$

Using the relations (2.3) and (2.7), we obtain:

$$\mathcal{J}_{0,t_r}^\varrho \Theta(t, x(t)) = \sum_{m=0}^r \frac{\alpha_{r,m} \delta^\varrho}{2\Gamma(1+\varrho)} \Theta(t_m, x_m),$$



and

$$\begin{aligned} \mathcal{J}_{0,t_r}^\varrho \left(\widehat{\Theta}(t, x(t)) \frac{dW(t)}{dt} \right) &= \int_0^{t_r} \frac{(t_r - \varsigma)^{\varrho-1}}{\Gamma(\varrho)} \widehat{\Theta}(\varsigma, x(\varsigma)) \omega(\varsigma) d\varsigma \\ &= \sum_{m=0}^r \frac{\alpha_{r,m} \delta^\varrho}{2\Gamma(1+\varrho)} \widehat{\Theta}(t_m, x_m) \omega_m, \end{aligned}$$

and

$$\begin{aligned} \mathcal{J}_{0,t_r}^\varrho \left(\widetilde{\Theta}(t, x(t)) \frac{d\beta^{H(t)}(t)}{dt} \right) &= \int_0^{t_r} \frac{(t_r - \varsigma)^{\varrho-1}}{\Gamma(\varrho)} \widetilde{\Theta}(\varsigma, x(\varsigma)) G^{H(t_r)}(\varsigma) d\varsigma \\ &= \sum_{m=0}^r \frac{\alpha_{r,m} \delta^\varrho}{2\Gamma(1+\varrho)} \widetilde{\Theta}(t_m, x_m) G_m^{H(t_m)}. \end{aligned}$$

Therefore,

$$\begin{aligned} x_r &= x_0 + \frac{\alpha_{r,r}}{2\Gamma(1+\varrho)} \left\{ \Theta(t_r, x_r) + \omega(t_r) \widehat{\Theta}(t_r, x_r) + G_r^{H(t_r)} \widetilde{\Theta}(t_r, x_r) \right\} \\ &+ \sum_{m=0}^{r-1} \frac{\alpha_{r,m}}{2\Gamma(1+\varrho)} \left\{ \Theta(t_m, x_m) + \omega(t_m) \widehat{\Theta}(t_m, x_m) + G_m^{H(t_m)} \widetilde{\Theta}(t_r, x_r) \right\}, \end{aligned} \tag{2.13}$$

where $\alpha_{r,m}$ is stated in (2.4) and $\alpha_{r,r} = 0$. Then,

$$x_r = x_0 + \sum_{m=0}^{r-1} \frac{\alpha_{r,m} \delta^\varrho}{2\Gamma(1+\varrho)} \left\{ \Theta(t_m, x_m) + \omega(t_m) \widehat{\Theta}(t_m, x_m) + G_m^{H(t_m)} \widetilde{\Theta}(t_m, x_m) \right\}.$$

3. ANALYSIS OF CONVERGENCE

We now analyze the convergence of the developed scheme for the approximate solution of Eq. (1.1). For this purpose, we consider the assumptions of Propositions 2.1 to 2.5. We assume $x(t) \in \mathbb{L}^2(\Omega, \mathcal{F}_t, \mathbb{P})$ and denote the exact and approximate solutions by x_m and $x(t_m)$, respectively, for $m = 0, 1, \dots, r$. Therefore, we define the error as:

$$\mathcal{E}_m = x_m - x(t_m), \quad m = 0, 1, \dots, r.$$

Let $\mathcal{E}_0 = 0$. Hence, according to 2.10, 2.11 and Hölder inequality, we obtain

$$\begin{aligned} \|\mathcal{E}_r\|_{ms}^2 &= \mathbb{E} \left[\left\| \int_0^{t_r} \frac{(t_r - \varsigma)^{\varrho-1}}{\Gamma(\varrho)} \cdot \Theta(\varsigma, x(\varsigma)) d\varsigma \right. \right. \\ &+ \int_0^{t_r} \frac{(t_r - \varsigma)^{\varrho-1}}{\Gamma(\varrho)} \cdot \widehat{\Theta}(\varsigma, x(\varsigma)) dW(\varsigma) + \int_0^{t_r} \frac{(t_r - \varsigma)^{\varrho-1}}{\Gamma(\varrho)} \cdot \widetilde{\Theta}(\varsigma, x(\varsigma)) d\beta^{H(t)}(\varsigma) \\ &- \left. \left. \sum_{m=0}^{r-1} \frac{\alpha_{r,m} \delta^\varrho}{2\Gamma(1+\varrho)} \left\{ \Theta(t_m, x_m) + \omega(t_m) \widehat{\Theta}(t_m, x_m) + G_m^{H(t_m)} \widetilde{\Theta}(t_m, x_m) \right\} \right\|^2 \right] \\ &\leq 3\mathbb{E} \left[\left\| \int_0^{t_r} \frac{(t_r - \varsigma)^{\varrho-1}}{\Gamma(\varrho)} \cdot \Theta(\varsigma, x(\varsigma)) d\varsigma - \sum_{m=0}^{r-1} \frac{\alpha_{r,m} \delta^\varrho}{2\Gamma(1+\varrho)} \Theta(t_m, x_m) \right\|^2 \right] \\ &+ 3\mathbb{E} \left[\left\| \int_0^{t_r} \frac{(t_r - \varsigma)^{\varrho-1}}{\Gamma(\varrho)} \cdot \widehat{\Theta}(\varsigma, x(\varsigma)) dW(\varsigma) - \sum_{m=0}^{r-1} \frac{\alpha_{r,m} \delta^\varrho}{2\Gamma(1+\varrho)} \omega(t_m) \widehat{\Theta}(t_m, x_m) \right\|^2 \right] \\ &+ 3\mathbb{E} \left[\left\| \int_0^{t_r} \frac{(t_r - \varsigma)^{\varrho-1}}{\Gamma(\varrho)} \cdot \widetilde{\Theta}(\varsigma, x(\varsigma)) d\beta^{H(t)}(\varsigma) - \sum_{m=0}^{r-1} \frac{\alpha_{r,m} \delta^\varrho}{2\Gamma(1+\varrho)} G_m^{H(t_m)} \widetilde{\Theta}(t_m, x_m) \right\|^2 \right]. \end{aligned}$$



In summary, we have:

$$\|\mathcal{E}_r\|_{ms}^2 \leq 3\mathbb{E}[\|\mathcal{E}_{r,\Theta}\|^2] + 3\mathbb{E}[\|\mathcal{E}_{r,\hat{\Theta}}\|^2] + 3\mathbb{E}[\|\mathcal{E}_{r,\hat{\Theta}}\|^2]. \quad (3.1)$$

Using Hölder's inequality and basic inequalities, we obtain

$$\begin{aligned} \mathbb{E}[\|\mathcal{E}_{r,\Theta}\|^2] &\leq 3\mathbb{E}\left[\left\|\int_0^{t_r} \frac{(t_r - \varsigma)^{\varrho-1}}{\Gamma(\varrho)} \cdot \Theta(\varsigma, x(\varsigma)) d\varsigma \sum_{m=0}^{r-1} \frac{\alpha_{r,m}\delta^\varrho}{2\Gamma(1+\varrho)} \Theta(t_m, x_m)\right\|^2\right] \\ &\quad + \frac{3r\delta^{2\varrho}}{4\Gamma^2(1+\varrho)} \sum_{m=0}^{r-2} \alpha_{r,m}^2 \mathbb{E}\left[\left\|\Theta(t_m, x(t_m)) - \Theta(t_m, x_m)\right\|^2\right] \\ &\quad + 3\alpha_{r,r}^2 \mathbb{E}[\|\Theta(t_r, x(t_r)) - \Theta(t_r, x_r)\|^2] \\ &\leq 3\left(\frac{r^{\varrho+2}\Xi}{\Gamma(\varrho+1)}\delta^{2+\varrho}\right)^2 + 3r\left(\frac{\Xi\theta_1}{16\Gamma(\varrho+1)}\delta^{2+\varrho}\right)^2 \sum_{m=0}^{r-1} \alpha_{r,m}^2, \end{aligned}$$

where

$$\sum_{m=0}^{r-1} \alpha_{r,m}^2 \leq r(1 + (\varrho - 2)r^{1-\varrho})^2 = r\phi^2.$$

Hence

$$\begin{aligned} \mathbb{E}[\|\mathcal{E}_{r,\Theta}\|^2] &\leq 3\left(\left(\frac{r^{\varrho+2}\Xi}{\Gamma(\varrho+1)}\right)^2 + r^2\phi^2\left(\frac{\Xi\theta_1}{16\Gamma(\varrho+1)}\right)^2\right)\delta^{4+2\varrho} \\ &\leq 3\tau_1\delta^{2\varrho+4}, \end{aligned}$$

where

$$\tau_1 = \left(\frac{r^{\varrho+2}\Xi + r\phi\theta_1\Xi}{\Gamma(\varrho+1)}\right)^2. \quad (3.2)$$

Similarly and assuming $\mathbb{E}[\|\omega(t)\|^2] = \delta^{-1}$ and $\mathbb{E}[\|G_r^{H(t_r)}\|^2] = \delta^{2H(t_r)-2}$, we have

$$\mathbb{E}[\|\mathcal{E}_{r,\hat{\Theta}}\|^2] \leq 3\left(\frac{r^{2\varrho-1}\Xi^2}{(2\varrho-1)\Gamma^2(\varrho)} + \left(\frac{\Xi r\phi\theta_2}{16\Gamma(\varrho+1)}\right)^2\right)\delta^{3+2\varrho} = 3\tau_2\delta^{3+2\varrho},$$

where

$$\tau_2 = \frac{r^{2\varrho-1}\Xi^2}{(2\varrho-1)\Gamma^2(\varrho)} + \left(\frac{\Xi r\phi\theta_2}{16\Gamma(\varrho+1)}\right)^2, \quad (3.3)$$

and

$$\begin{aligned} \mathbb{E}[\|\mathcal{E}_{r,\hat{\Theta}}\|^2] &\leq 3\left(\frac{H(t_r)r^{2\varrho+2H(t_r)-2}\Xi^2}{(2\varrho-1)\Gamma^2(\varrho)} + \left(\frac{\Xi r\phi\theta_3}{16\Gamma(\varrho+1)}\right)^2\right)\delta^{2+2\varrho+2H(t_r)} \\ &= 3\tau_3\delta^{2+2\varrho+2H(t_r)}, \end{aligned}$$

where

$$\tau_3 = \frac{H(t_r)r^{2\varrho+2H(t_r)-2}\Xi^2}{(2\varrho-1)\Gamma^2(\varrho)} + \left(\frac{\Xi r\phi\theta_3}{16\Gamma(\varrho+1)}\right)^2. \quad (3.4)$$

As a result, from (3.1), we gain

$$\|\mathcal{E}_r\|_{ms}^2 \leq 9\left(\tau_1\delta^{4+2\varrho} + \tau_2\delta^{3+2\varrho} + \tau_3\delta^{2+2\varrho+2H(t_r)}\right), \quad (3.5)$$

where τ_1 , τ_2 and τ_3 are presented in (3.2), (3.3), and (3.4), respectively.



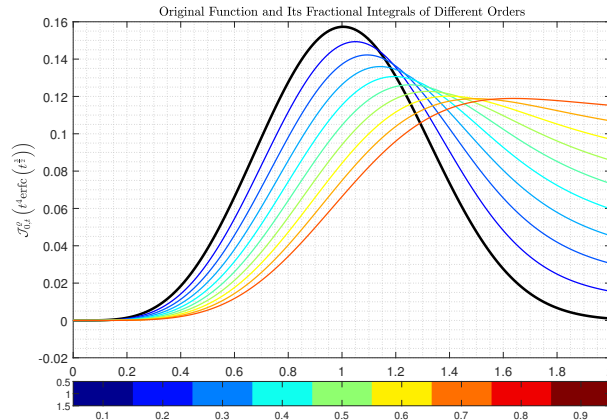


FIGURE 1. Fractional integrals of $t^4 \text{erfc}(t^{\frac{3}{2}})$ computed via Hermite interpolation method for different orders $\rho \in [0.1, 0.9]$ over $t \in [0, 2]$, with original function shown in black.

Subsequently

$$\|\mathcal{E}_r\|_{ms} \leq \tilde{\tau} \delta^{1+\varrho+H(t_r)}, \tag{3.6}$$

where $\tilde{\tau} = 3\sqrt{\tau_1 + \tau_2 + \tau_3}$ based on relations (3.2), (3.3), and (3.4), respectively. Therefore, the developed scheme has convergence order $\mathcal{O}(\delta^{1+\varrho+H(t_r)})$. This order shows faster convergence than IQS-algorithm [25] for variable Hurst indices.

4. ILLUSTRATIVE EXAMPLES

Now, the accuracy and computational efficiency of the presented approach are studied. For this purpose, the *expected mean absolute error* (EMAE) (\mathcal{E}_M) and the *convergence order* (ECO) are considered

$$\|\mathcal{E}_r\|_{ms} = \sum_{m=1}^r \frac{\mathbb{E}[\|AE_m^H\|]}{r}, \tag{4.1}$$

and

$$ECO = \log_\delta (\|\mathcal{E}_r\|_{ms}), \tag{4.2}$$

where $\mathbb{E}[\|AE_m^H\|]$ is expressed in (2.8), and r represents the number of interior mesh points. All the computational results are implemented with Maple v2019 running in an Intel (R) Core (TM) i3-8145U CPU @ 2.30 GHz machine. Furthermore, a comparison with the IQS-algorithm [25] is done.

Example 4.1. Let $x_\beta(t) = t^4 \text{erfc}(t^{\frac{3}{2}}) + \sigma G^{H(t)}(t)$ where $\text{erfc}(\cdot)$ is considered as complementary error function. We have

$$\mathcal{J}_{0,t}^\varrho \left(t^4 \text{erfc} \left(t^{\frac{3}{2}} \right) \right) = \frac{24t^{\varrho+4}}{\Gamma(\varrho+5)} - \frac{10395t^{\varrho+\frac{11}{2}} {}_4F_4 \left(\left[\frac{1}{2}, \frac{13}{6}, \frac{5}{2}, \frac{17}{6} \right], \left[\frac{3}{2}, \frac{5}{2} + \frac{\varrho}{3}, \frac{17}{6} + \frac{\varrho}{3}, \frac{13}{6} + \frac{\varrho}{3} \right]; -t^3 \right)}{32\Gamma(\varrho + \frac{13}{2})}, \tag{4.3}$$

where $\varrho > 0$ and generalized hypergeometric function is stated as ${}_sF_v(b_1, \dots, b_s; a_1, \dots, a_v; t)$.

Figure 1 demonstrates the effect of fractional integration on the function $t^4 \text{erfc}(t^{\frac{3}{2}})$, where the black curve represents the original function and the colored curves show its fractional integrals for orders $\rho \in [0.1, 0.9]$. As the fractional order ρ increases, the resulting curves exhibit greater smoothness and larger magnitudes while preserving the fundamental



TABLE 1. Comparison of $\|\mathcal{E}_r\|_{ms}$, ECO , and CPU time (based on sec.) for Example 4.1 with $\varrho \in (0, 3)$, $\sigma = 0.1$, $\delta = \{0.02, 0.01, 0.005\}$, and $H = 0.8 + 0.01t$ for $t \in [0, 3]$.

β	δ	IQS-algorithm [25]			Developed scheme		
		\mathcal{E}_M	ECO	$CPu\ time$	\mathcal{E}_M	ECO	$CPu\ time$
0.95	0.02	8.35×10^{-4}	1.812	2.015	4.96×10^{-4}	1.945	0.032
	0.01	4.17×10^{-4}	1.689	8.484	2.57×10^{-4}	1.795	0.064
	0.005	2.09×10^{-4}	1.600	38.375	1.34×10^{-4}	1.684	0.239
1.85	0.02	1.55×10^{-3}	2.110	56.140	5.22×10^{-6}	3.109	0.043
	0.01	7.71×10^{-4}	8.625	56.140	1.51×10^{-6}	2.910	0.095
	0.005	3.85×10^{-4}	37.265	56.140	4.35×10^{-7}	2.765	0.219
2.6	0.02	1.75×10^{-3}	1.623	2.156	4.61×10^{-6}	3.141	0.032
	0.01	8.65×10^{-4}	1.531	8.468	1.15×10^{-6}	2.969	0.083
	0.005	4.30×10^{-4}	1.463	37.172	2.86×10^{-7}	2.843	0.249

characteristics of the original function. The Hermite interpolation method employed here ensures numerical stability across the range of fractional orders, effectively illustrating the continuous nature of fractional integration between integer-order steps.

Based on the results presented in Table 1, the developed scheme demonstrates superior performance compared to the IQS-algorithm [25] across most tested parameters. For varying values of β (0.95, 1.85, and 2.6) and δ (0.02, 0.01, and 0.005), the new method consistently achieves lower error values (\mathcal{E}_M) for $\beta \geq 1.85$, higher experimental convergence orders (ECO), and significantly reduced computational times. The improvements are particularly pronounced for higher β values, where the developed scheme reduces errors by several orders of magnitude while maintaining substantially higher ECO values. As δ decreases, both methods show improved accuracy, but the developed scheme maintains a significant advantage in computational efficiency, with speed-ups of several orders of magnitude. These results indicate that the proposed method offers enhanced accuracy (for $\beta \geq 1.85$), faster convergence rates, and dramatically improved computational efficiency compared to the IQS-algorithm, particularly for problems characterized by higher β values.

4.1. Application: Fractional Extended Heston Models with Interest Rate Driven by Variable-Order Brownian Motions. To address economic challenges, numerous mathematical models have been developed. One prominent example is the Heston model [17], which was introduced to analyze sharp market volatility. The model is expressed as follows:

$$\begin{cases} \mathcal{D}_t S(t) = RS(t) + S(t)\sqrt{V(t)}\frac{d\beta_1}{dt}, \\ \mathcal{D}_t V(t) = \kappa_V(\theta_V - V(t)) + \sigma_V\sqrt{V(t)}\frac{d\beta_2}{dt}, \\ S(0) = S_0, \quad V(0) = V_0, \end{cases} \quad (4.4)$$

where, $S(t)$ and $V(t)$ represent the stock price and its return variance at time t , respectively. The risk-free rate is denoted by r , θ_V represents the long-term volatility mean, and κ_V denotes the rate at which volatility reverts to θ_V . The terms β_1 and β_2 are Brownian motions.

To enhance the classical Heston model, fractional calculus can be incorporated, leading to fractional extended Heston models where variable-order fractional Brownian motions drive the interest rates. These models account for the time-dependent nature of market volatility more accurately, allowing for a better fit to empirical data.

Fractional differential operators extend traditional differential equations to include memory effects and non-local dynamics, reflecting more complex market behaviors. The use of fractional Brownian motion $\beta_H(t)$ with Hurst parameter H offers a more flexible framework for modeling asset price dynamics, capturing long-range dependence and self-similarity observed in financial time series.



The impact of volatility on financial markets has been extensively studied through various stochastic models. Authors have explored the implications of these models on pricing and risk management [7, 8, 15, 31]. These investigations highlight the significance of incorporating stochastic volatility in developing robust financial instruments and strategies. By integrating variable-order Brownian motions and fractional calculus, modern Heston models provide a comprehensive tool for analyzing complex financial phenomena, ensuring more accurate risk assessment and pricing in volatile markets.

In [30], the fractional Heston model (nHm) was studied as

$$\begin{cases} {}^C \mathcal{D}_{0,t}^{\varrho_1} S(t) = RS(t) + S(t)\sqrt{V(t)}\frac{d\beta_1}{dt}, \\ {}^C \mathcal{D}_{0,t}^{\varrho_2} V(t) = \kappa_V(\theta_V - V(t)) + \sigma_V\sqrt{V(t)}\frac{d\beta_2}{dt}, \\ S(0) = S_0, \quad V(0) = V_0, \end{cases} \quad (4.5)$$

where $\varrho_1, \varrho_2 \in (\frac{1}{2}, 1)$.

In this study, we consider the fractional extended Heston models with interest rates as follows:

$$\begin{cases} {}^C \mathcal{D}_{0,t}^{\varrho_1} S(t) = R(t)S(t) + S(t)\sqrt{V(t)}\frac{d\beta_1}{dt}, \\ {}^C \mathcal{D}_{0,t}^{\varrho_2} V(t) = \kappa_V(\theta_V - V(t)) + \sigma_V\sqrt{V(t)}\frac{d\beta_2}{dt}, \\ {}^C \mathcal{D}_{0,t}^{\varrho_3} R(t) = \kappa_R(\theta_R - R(t)) + \sigma_R(R(t))^p\frac{d\beta^{H(t)}(t)}{dt}, \\ S(0) = S_0, \quad V(0) = V_0, \quad R(0) = R_0, \end{cases} \quad (4.6)$$

where $\varrho_1, \varrho_2, \varrho_3 \in (\frac{1}{2}, 1)$ and $H \in (\frac{1}{2}, 1)$. This system is referred to as the fractional Heston-Hull-White model (HHW-VBM) for $p = 0$ and the fractional Heston-Cox-Ingersoll-Ross model (HCIR-VBM) for $p = 0.5$. The interest rate at time t is denoted by $R(t)$; θ_R represents the long-term mean of the interest rate; and κ_R denotes the speed of adjustment to θ_R . The term $\beta^{H(t)}$ denotes a variable-order Brownian motion. It is worth noting that $\frac{d\beta_1}{dt} \cdot \frac{d\beta_2}{dt} = \rho_1$, $\frac{d\beta_1}{dt} \cdot \frac{d\beta^{H(t)}}{dt} = \rho_2$ and $\frac{d\beta_2}{dt} \cdot \frac{d\beta^{H(t)}}{dt} = \rho_3$, where $\rho_1, \rho_2, \rho_3 \in [-1, 1]$ are correlation coefficients. The system (4.6) can then be rewritten as follows:

$$\begin{pmatrix} {}^C \mathcal{D}_{0,t}^{\varrho_1} S(t) \\ {}^C \mathcal{D}_{0,t}^{\varrho_2} V(t) \\ {}^C \mathcal{D}_{0,t}^{\varrho_3} R(t) \end{pmatrix} = \begin{pmatrix} R(t)S(t) \\ \kappa_V(\theta_V - V(t)) \\ \kappa_R(\theta_R - R(t)) \end{pmatrix} + \begin{pmatrix} S(t)\sqrt{V(t)} & 0 & 0 \\ \rho_1\sigma_V\sqrt{V(t)} & \sigma_V\sqrt{(1-\rho_1^2)V(t)} & 0 \\ \rho_2\sigma_R(R(t))^p & \frac{\rho_3-\rho_1\rho_2}{\sqrt{1-\rho_1^2}}\sigma_R(R(t))^p & \sqrt{1-\rho_2^2 - \left(\frac{\rho_3-\rho_1\rho_2}{\sqrt{1-\rho_1^2}}\right)^2\sigma_R(R(t))^p} \end{pmatrix} \begin{pmatrix} \frac{d\beta_1}{dt} \\ \frac{d\beta_2}{dt} \\ \frac{d\beta^{H(t)}}{dt} \end{pmatrix}, \quad (4.7)$$

We employ a discretization scheme based on the developed method to estimate the price behavior of the S&P 500 index during the interval from 03/01/1995 to 09/11/1999, covering 1227 workdays. Consequently, we have $r = 1227$ equally spaced mesh points. The initial values are set as $S(0) = 459.2$, $V(0) = 0.00411$, and $R(0) = 1.05$. It is worth noting that these values in Eq. (4.7) were calibrated using historical S&P 500 data from 1995–1999. Additionally, using a genetic algorithm, we determine the optimal fractional orders to be $\varrho_1 = 0.8816$, $\varrho_2 = 0.9292$, and $\varrho_3 = 0.8723$. The parameter values are given by $\kappa_V = 2.75$, $\theta_V = 0.035$, $\sigma_V = 0.425$, $\kappa_R = 0.044$, $\theta_R = 0.08$, $\sigma_R = 0.0065$, $\rho_1 = -0.4644$, $\rho_2 = 0$, and $\rho_3 = -0.8344$.

To evaluate the performance of the proposed method and the extended Heston model, we utilize several well-known performance review criteria. Descriptions of these criteria are provided in Table 2. In this table, c and N represent the number of parameters and observations in the model, respectively [14].

According to Table 2, the results are analyzed in Table 3. Table 3 presents a comprehensive comparison of performance review criteria for various fractional Heston models, utilizing our developed scheme with $n = 1227$ over the interval $t \in [0, 1]$. The results clearly demonstrate the superiority of models incorporating time-varying Hurst functions, particularly the HCIR-VBM model with $H_2(t)$. This model consistently outperforms others across all criteria,



TABLE 2. Key Performance Evaluation Metrics

Metric	Calculation Method
Absolute Error (AE)	$ (actual)_m - (estimated)_m , \quad m = 1, \dots, r$
Mean Absolute Error (MAE)	$\frac{1}{r} \sum_{m=1}^r AE_m$
Sum of Squared Residuals (SSR)	$\sum_{m=1}^r (AE_m)^2$
Root Mean Square Error (RMSE)	$\sqrt{\frac{SSR}{N-c-1}}$
Bayesian Information Criterion (BIC)	$N \ln\left(\frac{SSR}{N}\right) + c \ln(N)$
Akaike Information Criterion (AIC)	$N \ln(SSR) + 2c$

TABLE 3. Comparison of performance review criteria of fractional Heston models using developed scheme with $n = 1227$ in $t \in [0, 1]$.

Model	MAE	RSS	RMSE	BIC	AIC
nHm	44.95	4.7157×10^6	1.3501×10^5	10156.67	18849.18
HHW-VBM ($H_1(t)$)	54.10	6.5150×10^6	1.8668×10^5	10566.53	19249.47
HHW-VBM ($H_2(t)$)	38.89	3.2546×10^6	9.3256×10^4	9715.64	18398.58
HCIR-VBM ($H_1(t)$)	41.61	3.7064×10^6	1.0620×10^5	9875.01	18557.95
HCIR-VBM ($H_2(t)$)	38.85	3.2484×10^6	9.3078×10^4	9713.30	18396.24

exhibiting the lowest MAE (38.85), RSS (3.2484×10^6), RMSE (9.3078×10^4), BIC (9713.30), and AIC (18396.24). Notably, both HCIR-VBM and HHW-VBM models using $H_2(t)$ show significant improvements over their counterparts using the constant Hurst parameter $H_1(t)$, emphasizing the advantages of time-varying fractional behavior. The nHm model demonstrates intermediate performance, while the HHW-VBM model with $H_1(t)$ consistently ranks lowest. These findings strongly support the efficacy of our developed scheme and highlight the enhanced accuracy and efficiency achieved through the incorporation of time-varying Hurst functions in fractional Heston models.

To further evaluate performance, we examine statistical indicators (SIs). It is important to note that standard mathematical methods cannot yield analytical solutions for the SBFDE. Therefore, we employ the upper 95% confidence interval (CI) to predict the behavior of sample trajectories for approximated solutions in fractional stochastic models [11, 27]. Table 4 presents the approximated SI values based on 30 simulated trajectories at $T = 1$ ($n=1227$). The statistical indicators presented in Table 4 lead to several significant conclusions regarding the performance of various fractional Heston models. The HCIR-VBM model, utilizing the time-varying Hurst function $H_2(t) = 0.98 - 0.08|\sin(\sqrt{t})|$, exhibits superior stability and consistency, as demonstrated by its lowest standard deviation (10.92), the narrowest 95% confidence interval [1380.9, 1417.6], and a perfectly symmetric distribution (skewness = 0). In contrast, the nHm model shows the highest variability, characterized by the largest standard deviation (263.5) and the widest confidence interval [895.1, 1928.2]. Notably, both the HHW-VBM and HCIR-VBM models that use the time-varying Hurst function H_2 exhibit significantly lower variability compared to their counterparts with the constant Hurst parameter H_1 . This is reflected in their reduced standard deviations and narrower confidence intervals. All models demonstrate platykurtic distributions ($kurtosis < 3$) and near-symmetric behavior (skewness close to 0). These findings strongly indicate the superiority of variable-fBm over fixed-fBm in fractional Heston models, with the HCIR-VBM (H_2) model emerging as the most effective among those evaluated.

Our analysis demonstrates that fractional Heston models with variable-fBm exhibit superior performance compared to those with fixed-fBm. Furthermore, examination of the SIs indicates that the HCIR-VBM model driven by $H_2(t) = 0.98 - 0.08|\sin(\sqrt{t})|$ yields the most favorable results among the tested models.

To evaluate the extended fractional Heston model, we analyze both experimental and numerical solutions for the fractional model (4.7) at $p = 0$ and $p = 0.5$, as illustrated in Figure 2. This figure examines the Hurst indexes, specifically $H_1(t) = 0.7127$ and $H_2(t) = 0.98 - 0.08|\sin(\sqrt{t})|$. The experimental results are represented by red circles.



TABLE 4. Comparison of SIs of fractional Heston models of the 30 simulated trajectories using developed scheme with $n = 1227$ in $t \in [0, 1]$.

SIs	nHm	HHW-VBM (H_1)	HHW-VBM (H_2)	HCIR-VBM (H_1)	HCIR-VBM (H_2)
Mean	1411.6	1536.3	1496.6	1435.9	1399.3
Median	1434.4	1536.3	1497.0	1436.0	1399.3
First quartile	1235.7	1332.5	1413.7	1309.1	1388.9
Third quartile	1596.35	1740.8	1580.1	1562.3	1410.4
Skewness	-0.151	-0.007	0.116	0.1323	0.000
Kurtosis	2.640	2.000	2.500	2.323	2.863
Standard deviation	263.5	203.8	83.552	126.43	10.92
95% CI	[895.1, 1928.2]	[1193.7, 1878.8]	[1356.2, 1636.9]	[1223.5, 1648.3]	[1380.9, 1417.6]

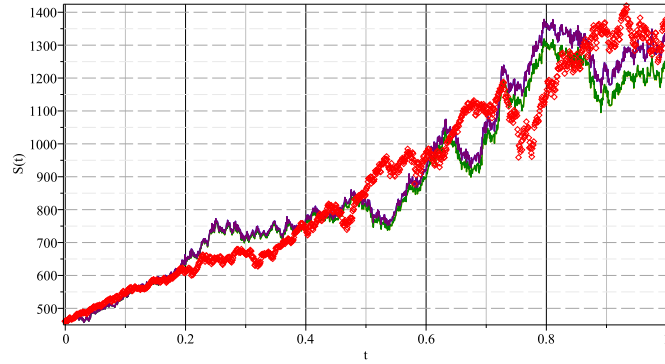


FIGURE 2. The experimental and numerical results stock-price ($S(t)$), for model (4.7) for $p = \{0, 0.5\}$ and $H(t) = \{0.7127, 0.98 - 0.08|\sin(\sqrt{t})|\}$ with $r = 1227$. Experimental (red circle), HHW-VBM- H_1 (black line), HHW-VBM- H_2 (blue line), HCIR-VBM- H_1 (green line), HCIR-VBM- H_2 (purple line)

These findings highlight the influence of Hurst indexes and different values of p on the parameters $\varrho_1 = 0.8816$, $\varrho_2 = 0.9292$, and $\varrho_3 = 0.8723$ with $r = 1227$.

In Figure 3, we display the curves of statistical indicators (SIs) for the fractional model (4.7) using the proposed scheme with $T = 1$. The parameters used are $\varrho_1 = 0.8816$, $\varrho_2 = 0.9292$, and $\varrho_3 = 0.8723$ with $r = 1227$ and $H(t) = \{0.7127, 0.98 - 0.08|\sin(\sqrt{t})|\}$. The results are shown across 30 trajectories, including the 95% confidence interval, first and third quartiles, and the point-by-point sample mean for t in the range $[0, 1]$.

5. CONCLUSION

The research presented an explicit approximation methodology for solving fractional extended Heston models incorporating interest rate in variable-order Brownian motions. Through the integration of trapezoidal quadrature for fractional order integral operators with stochastic fractional differential equations in fractional Brownian motion, a robust computational framework was established. Comparative analysis between the numerical results for fractional order integral operators and the IQS-algorithm revealed significant insights across three key metrics: error magnitude, computational efficiency, and processing time.

The implementation of the developed algorithm in analyzing fractional extended Heston models yielded comprehensive results across diverse Hurst index values, with optimal fractional orders determined through Genetic Algorithms. This systematic investigation provided valuable insights into the stochastic behaviors of these models, while statistical indicators validated the efficiency and reliability of the proposed methodology.

The promising results demonstrate the algorithm’s potential for solving fractional extended Heston models and suggest broader applications within stochastic modeling. This method can predict stock prices faster in volatile markets, as shown in the comparative analysis. This work contributes to bridging theoretical foundations with practical



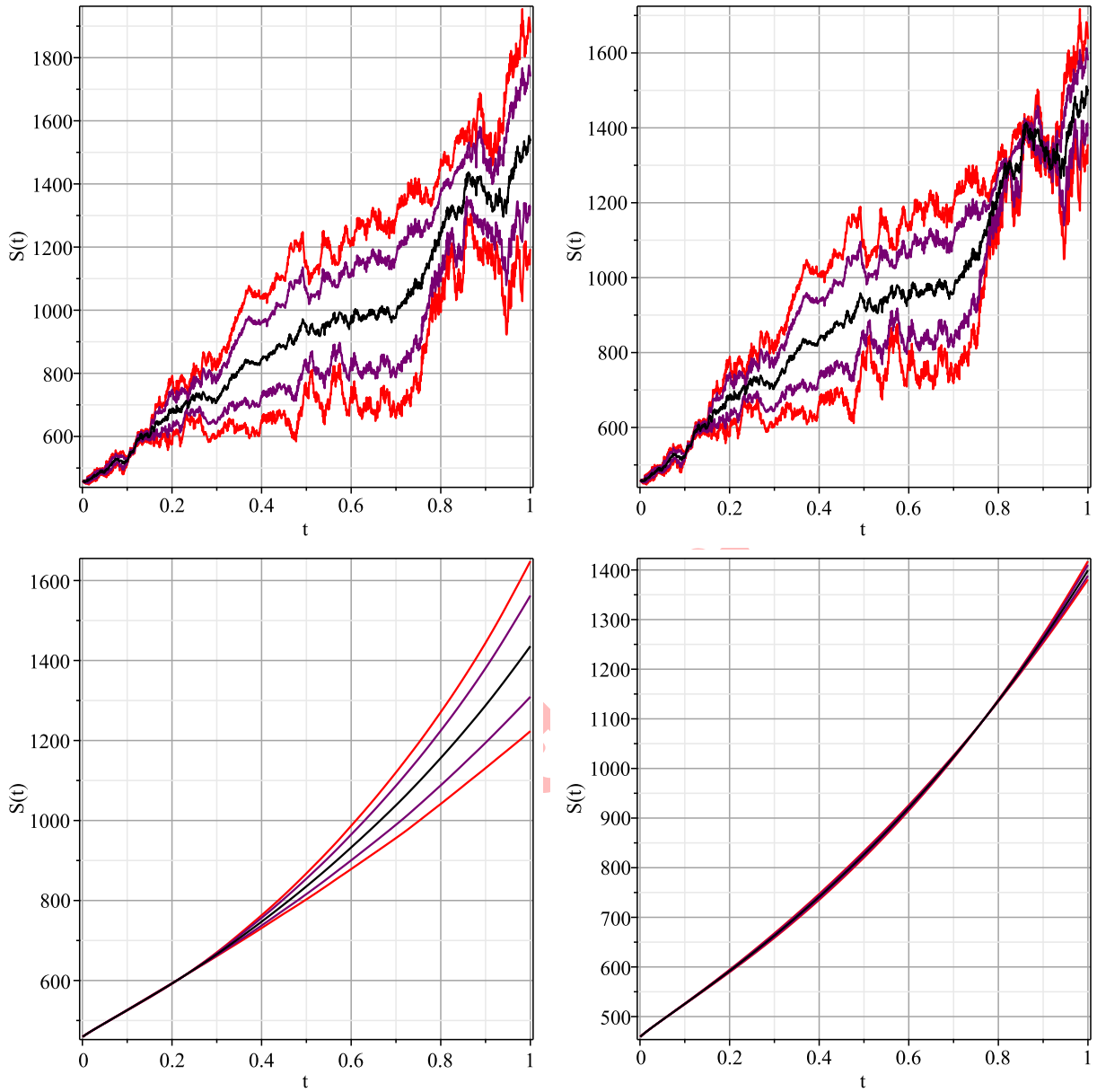


FIGURE 3. Comparison of stock price dynamics $S(t)$ over time for model (4.7) that left panels use $H_1 = 0.7127$ and right panels use $H_2 = 0.98 - 0.08|\sin(\sqrt{t})|$ for both HHW-VBM and HCIR-VBM models. Results are based on 30 simulated trajectories, displaying the point-wise sample mean (black), first and third quartiles (purple), and 95% confidence interval (red).

applications in financial modeling, combining mathematical rigor with computational efficiency. The implications extend to enhanced understanding of complex financial systems and improved risk assessment methodologies. Future research directions may explore applications to other stochastic fractional differential equation problems, incorporation of additional market factors, investigation of alternative optimization techniques, and analysis of model performance under extreme market conditions. This expansion could further validate the methodology's robustness and extend its



practical utility in financial modeling and risk assessment. Moreover, future work can include testing the method on models with sudden market jumps or using other numerical methods for the stochastic differential equations.

DECLARATIONS

Ethical Approval. Not applicable. This study is theoretical and computational in nature and does not involve human or animal subjects.

Availability of Supporting Data. No datasets were generated or analyzed during this study, as it focuses on numerical simulations and theoretical analysis. All results are presented within the manuscript.

Competing Interests. The authors, Z. Tokasi, M. Ilie, B. Parsa Moghaddam, and K. Hosseini, declare no competing interests that could influence the research presented in this manuscript.

Funding. No funding was received for this research.

Authors' Contributions. Z. Tokasi designed the numerical methodology, performed computational experiments, and drafted the manuscript. M. Ilie conceptualized the study, developed the theoretical framework, and critically revised the manuscript. B. Parsa Moghaddam contributed to the convergence analysis, provided technical expertise, and reviewed the manuscript. K. Hosseini assisted in the application of fractional calculus to Heston models, refined the theoretical analysis, and revised the manuscript. All authors read and approved the final manuscript.

Acknowledgments. No acknowledgments to report at this time.

REFERENCES

- [1] W. M. Abd-Elhameed and M. M. Alsuyuti, *Numerical treatment of multi-term fractional differential equations via new kind of generalized Chebyshev polynomials*, *Fractal and Fractional*, 7(1) (2023), 74.
- [2] H. M. Ahmed, *Approximate controllability via resolvent operators of Sobolev-type fractional stochastic integrodifferential equations with fractional Brownian motion and Poisson jumps*, *Bulletin of the Iranian Mathematical Society*, 45(4) (2018), 1045–1059.
- [3] A. S. Ahmed, *Existence and uniqueness of mild solutions to neutral impulsive fractional stochastic delay differential equations driven by both Brownian motion and fractional Brownian motion*, *Differential Equations and Applications*, (3) (2022), 433–446.
- [4] I. Ali and S. U. Khan, *A dynamic competition analysis of stochastic fractional differential equation arising in finance via pseudospectral method*, *Mathematics*, 11(6) (2023), 1328.
- [5] N. Ayazi, P. Mokhtary, and B. P. Moghaddam, *Efficiently solving fractional delay differential equations of variable order via an adjusted spectral element approach*, *Chaos, Solitons & Fractals*, 181 (2024), 114635.
- [6] F. G. Bahador, P. Mokhtary, and M. Lakestani, *Mixed Poisson-Gaussian noise reduction using a time-space fractional differential equations*, *Information Sciences*, 647 (2023), 119417.
- [7] S. Bayad, K. Hilal, and A. E. Hajaji, *Applied Mathematics and Modelling in Finance*, Marketing and Economics, Springer, (2024), 197–206.
- [8] S. Boyarchenko and S. Levendorskil, *American options in the Heston model with stochastic interest rate and its generalizations*, *Applied Mathematical Finance*, 20(1) (2013), 26–49.
- [9] M. Caputo, *Linear models of dissipation whose Q is almost frequency independent-II*, *Geo335 physical Journal International*, 13(5) (1967), 529–539.
- [10] M. Caputo, *Elasticità e dissipazione*, Zanichelli, Bologna, Italy, 1969.
- [11] C. Chatfield, *Statistics for technology*, Routledge, 2018.
- [12] A. T. Dincel, S. N. T. Polat, and P. Sahin, *Hermite wavelet method for nonlinear fractional differential equations*, *Fractal and Fractional*, 7(5) (2023), 346.
- [13] X. L. Ding and J. Nieto, *Analytical solutions for multi-time scale fractional stochastic differential equations driven by fractional Brownian motion and their applications*, *Entropy*, 20(1) (2018), 63.
- [14] N. G. Hossein-Zadeh, *Application of growth models to describe the lactation curves for testday milk production in Holstein cows*, *Journal of Applied Animal Research*, 45(1) (2016), 145–151.



- [15] L. A. Grzelak and C. W. Oosterlee, *On the Heston model with stochastic interest rates*, SIAM Journal on Financial Mathematics, 2(1) (2011), 255–286.
- [16] F. Haddouchi, *On the existence and uniqueness of solutions for fractional differential equations with nonlocal multi-point boundary conditions*, Differential Equations and Applications, (3) (2021), 227–242.
- [17] S. L. Heston, *A closed-form solution for options with stochastic volatility with applications to bond and currency options*, Review of Financial Studies, 6(2) (1993), 327–343.
- [18] M. Heydari, M. Mahmoudi, A. Shakiba, and Z. Avazzadeh, *Chebyshev cardinal wavelets and their application in solving nonlinear stochastic differential equations with fractional Brownian motion*, Communications in Nonlinear Science and Numerical Simulation, 64 (2018), 98–121.
- [19] M. Heydari, Z. Avazzadeh, and M. Mahmoudi, *Chebyshev cardinal wavelets for nonlinear stochastic differential equations driven with variable-order fractional Brownian motion*, Chaos, Solitons & Fractals, 124 (2019), 105–124.
- [20] S. R. Kaafi, E. Hesameddini, and P. Mokhtaryi, *A novel algorithm and its convergence analysis for solving the generalized Abel integral equations through fractional calculus*, Asian-European Journal of Mathematics, 16(09) (2023), 2350158.
- [21] W. Liu and J. Luo, *Neutral stochastic differential equations driven by Brownian motion and fractional Brownian motion in a Hilbert space*, Publicationes Mathematicae Debrecen, 87(1-2) (2015), 235–253.
- [22] M. R. Mahmoudi, *A computational technique to classify several fractional Brownian motion processes*, Chaos, Solitons & Fractals, 150 (2021), 111152.
- [23] B. P. Moghaddam, L. Zhang, A. M. Lopes, J. A. T. Machado, and Z. S. Mostaghim, *Sufficient conditions for existence and uniqueness of fractional stochastic delay differential equations*, Stochastics, 92(3) (2019), 379–396.
- [24] B. P. Moghaddam, Z. S. Mostaghim, and E. Hashemi Zadeh, *Computational method for fractional-order stochastic delay differential equations*, Journal of New Researches in Mathematics, 6(26) (2021), 19–31.
- [25] B. P. Moghaddam, Z. S. Mostaghim, A. Pantelous, and J. T. Machado, *An integro quadratic splinebased scheme for solving nonlinear fractional stochastic differential equations with constant time delay*, Communications in Nonlinear Science and Numerical Simulation, 92 (2021), 105475.
- [26] B. P. Moghaddam, A. Dabiri, Z. S. Mostaghim, and Z. Moniri, *Numerical solution of fractional dynamical systems with impulsive effects*, International Journal of Modern Physics C, 34(01) (2022).
- [27] B. P. Moghaddam, M. Pishbin, Z. S. Mostaghim, O. S. Iyiola, A. Galhano, and A. M. Lopes, *A numerical algorithm for solving nonlocal nonlinear stochastic delayed systems with variableorder fractional Brownian noise*, Fractal and Fractional, 7(4) (2023), 293.
- [28] Z. Moniri, A. Babaei, and B. P. Moghaddam, *Robust numerical framework for simulating 2D fractional time-space stochastic diffusion equation driven by spatio-temporal noise: L1-FFT hybrid approach*, Communications in Nonlinear Science and Numerical Simulation, 146 (2025), 108791.
- [29] Z. Moniri, A. Babaei, and B. P. Moghaddam, *Numerical exploration of pollutant transport using stochastic fractional diffusion and Karhunen-Loève expansion*, Iranian Journal of Numerical Analysis and Optimization, (2025).
- [30] Z. S. Mostaghim, B. P. Moghaddam, and H. S. Haghgozar, *Computational technique for simulating variable-order fractional Heston model with application in US stock market*, Mathematical Sciences, 12 (2018), 277–283.
- [31] L. Perotti and L. A. Grzelak, *On pricing of discrete asian and lookback options under the Heston model*, International Journal of Computer Mathematics, (2024), 1–30.
- [32] F. Rihan and H. Alsakaji, *Dynamics of a stochastic delay differential model for COVID-19 infection with asymptomatic infected and interacting people: Case study in the UAE*, Results in Physics, 28 (2021), 104658.
- [33] A. Y. A. Salamooni and D. D. Pawar, *Existence and uniqueness of nonlocal boundary conditions for Hilfer-Hadamard-type fractional differential equations*, Advances in Difference Equations, 2021(1) (2021).
- [34] S. G. Samko, A. A. Kilbas, and O. I. Marichev, *Fractional Integrals and Derivatives: Theory and Applications*, Gordon & Breach Sci. Publishers, 1993.
- [35] A. Shahnazi-Pour, B. P. Moghaddam, and A. Babaei, *Numerical simulation of the Hurst index of solutions of fractional stochastic dynamical systems driven by fractional Brownian motion*, Journal of Computational and Applied Mathematics, 386 (2021), 113210.



- [36] A. Shahnazi-Pour, B. P. Moghaddam, and A. Babaei, *A computational technique for nonlinear nonlocal stochastic dynamical systems with variable order fractional Brownian noise*, *Journal of Applied Nonlinear Dynamics*, *12*(1) (2023), 75–85.
- [37] H. Sheng, H. Sun, Y. Chen, and T. Qiu, *Synthesis of multifractional Gaussian noises based on variable-order fractional operators*, *Signal Processing*, *91*(7) (2011), 1645–1650.
- [38] Q. Yang, D. Chen, T. Zhao, and Y. Chen, *Fractional calculus in image processing: A review*, *Fractional Calculus and Applied Analysis*, *19*(5) (2016), 1222–1249.
- [39] C. Zuniga-Aguilar, J. Gomez-Aguilar, R. Escobar-Jimenez, and H. Romero-Ugalde, *A novel method to solve variable-order fractional delay differential equations based in lagrange interpolations*, *Chaos, Solitons and Fractals*, *126* (2019), 266–282.

Uncorrected Proof

